



Tensile Properties and Serrated Flow Behavior of As-Cast CoCrFeMnNi High-Entropy Alloy at Room and Elevated Temperatures

Jeoung Han Kim¹ · Young Sang Na²

Received: 1 September 2018 / Accepted: 30 September 2018 / Published online: 25 October 2018
© The Korean Institute of Metals and Materials 2018

Abstract

The tensile properties and serrated flow behavior of as-cast CoCrFeMnNi high-entropy alloy were examined over a wide range of temperatures. Tensile elongations were higher at 22 °C than at high temperatures above 700 °C. With the increase in the temperature from 500 to 700 °C, distinct serration flows occurred and evolved in the sequence of type A, type B, and type C serrations. Anisotropy in the tensile properties and serrated flow was identified. The average stress drop amplitude in the serrated flow was generally higher when tensile loading was applied perpendicular to the columnar grain growth direction. Moreover, 700 °C, the strain increment required for subsequent stress drops was significantly lower when tensile loading was applied perpendicular to the columnar grain growth direction. The start and finish temperatures of serration flow were slightly higher in as-cast HEA by 100–200 °C compared to those in wrought HEA.

Keywords Stress/strain measurements · Other metallic alloys · Casting methods · Grains and interfaces, plasticity

1 Introduction

The design strategy of high-entropy alloys (HEAs) is based on the mixing of five or more elements in equiatomic or near-equiatomic concentrations such that the high configurational entropy ΔS_{conf} promotes single-phase solid solution formation [1]. Owing to their remarkable damage tolerance at a tensile strength of approximately 1 GPa and with a fracture toughness exceeding 200 MPa m^{1/2} [2], HEAs have drawn significant interest. In particular, the face-centered cubic (FCC) CoCrFeMnNi HEA exhibits improvements in terms of both strength and ductility [3–5] owing to deformation twinning at low temperatures. Hence, HEAs are expected to replace conventional austenitic steel for cryogenic applications. HEAs are often produced using vacuum arc melting followed by drop-casting into a copper mold [6–8]. After homogenization

at a temperature above 1000 °C, the alloys are hot-rolled to break down their cast structures and obtain a recrystallized microstructure [9, 10]. HEA materials have been produced by hot rolling at temperatures in the range of 800–1000 °C [11, 12] and by cold rolling without any intermediate annealing [7, 13, 14].

The Portevin–Le Chatelier (PLC) effect is a well-known plastic instability phenomenon frequently observed in many metallic materials. One of the key characteristics of the PLC effect is the presence of “serrated flow” in the stress–strain curve within certain ranges of temperature and strain rate [15]. During the plastic deformation process, such an unstable plastic flow leads to inhomogeneous strain localization [16]. Moreover, the plastic instability frequently results in samples with rippled surfaces, which are undesirable in industrial processes [17]. Many FCC structured HEAs have been reported to exhibit a distinct serrated flow behavior during deformation at temperatures in the range of approximately 400–600 °C. Fu et al. [18] studied the serrated flow behavior of CoCrFeMnNi HEA and determined the activation energies for the serrated flow in different temperature ranges. Carroll et al. [19] developed an analytical model explaining the serrated flow in terms of the slip avalanche at slipping weak spots and slip statistics. They related the plastic behavior with the temperature, strain

✉ Jeoung Han Kim
jh.kim@hanbat.ac.kr

✉ Young Sang Na
nys1664@kims.re.kr

¹ Department of Materials Science and Engineering, Hanbat National University, Daejeon 34158, Republic of Korea

² Titanium Department, Korea Institute of Materials Science, Changwon 51508, Republic of Korea

Fig. 1 Tensile sample machining direction. Ellipsoids in blue represent the growth shape of the columnar grains. H and W_s indicate the sample machining directions. (Color figure online)

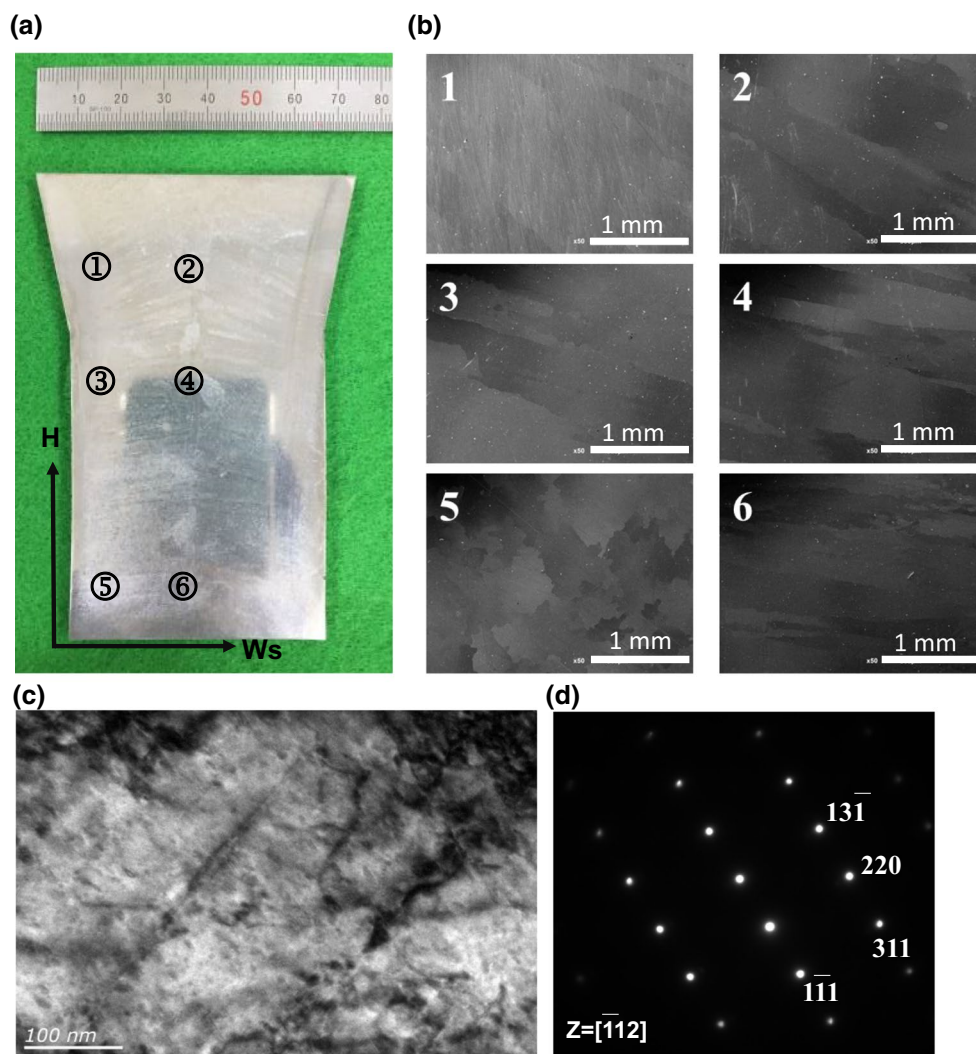
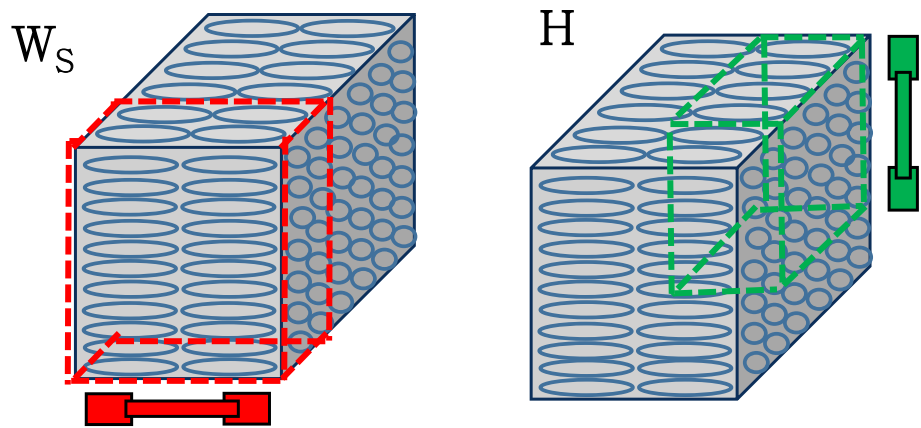


Fig. 2 **a** Macroscopic structure of as-cast CoCrFeMnNi high-entropy alloy block, and **b** SEM images of the different regions shown in **(a)**. **c**, **d** TEM image and corresponding selected area diffraction pattern

showing typical microstructure of as-cast CoCrFeMnNi high-entropy alloy. H and W_s in **(a)** indicate the sample machining directions

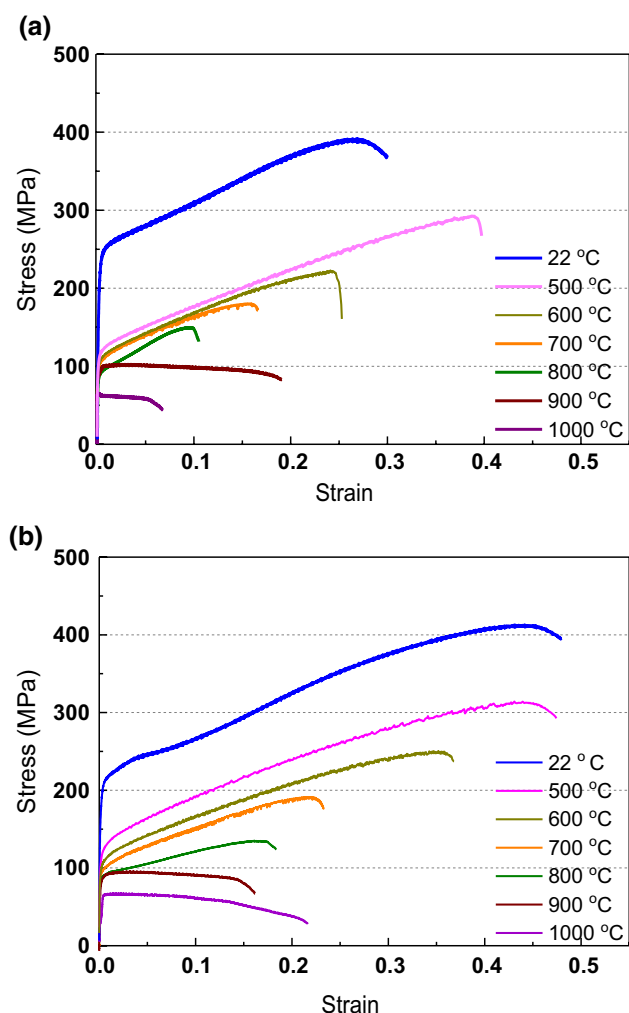


Fig. 3 Representative engineering stress–strain curves of the ascast CoCrFeMnNi alloy at low and high temperatures. Initial strain rate is 10^{-3} s^{-1}

rate, and material composition. However, most of the aforementioned studies focused on wrought HEA alloys, which either have a fine grain size (generally less than several tens of microns) or are dendrite-free after the cast structure solidifies. The first step in preparing wrought CoCrFeMnNi is to break down the dendritic cast structure of the alloy ingot. Therefore, it is necessary to investigate the plastic behavior of HEAs in the as-cast state. In this work, we investigated the tensile properties and related serrated flow of an equiatomic FCC CoCrFeMnNi HEA. The effect of loading direction on the plastic flow was studied. Finally, the serration behavior of the as-cast HEA was compared with that of wrought HEA.

2 Materials and Experimental Methods

Ingots (8 kg) with nominal compositions were fabricated by vacuum induction melting. The melt was poured into a Y-block graphite mold to minimize the size of the shrinkage cavity in the bottom part of the ingot (the dimensions of this part were $110 \times 60 \times 80 \text{ mm}$). The as-cast HEA was homogenized at $1000 \text{ }^\circ\text{C}$ for 6 h, furnace cooled to $700 \text{ }^\circ\text{C}$, and subsequently air cooled. The chemical composition of the ingot measured using inductively coupled plasma optical emission spectrometry was 21.5Co–18.4Cr–20.1Fe–18.4Mn–21.2Ni–0.2Si–0.05C–0.01N (in wt%). To investigate the mechanical properties and deformation behavior of the as-cast ingots, uniaxial tensile tests (ASTM E8) were conducted at temperatures ranging from 22 to $1000 \text{ }^\circ\text{C}$ with a strain rate of $1 \times 10^{-3} \text{ s}^{-1}$. The tensile test was conducted with UT-100E model with SL400 load cell. Maximum load cell capacities were 100 and 20 kN for room temperature and high temperature tests, respectively. To examine the anisotropy, the tensile test specimens were machined along two directions of the as-cast ingot, W_S and H (Figs. 1, 2a).

The microstructures were examined at the gauge sections of the as-cast tensile test specimens before straining. Scanning electron microscope (SEM) images of the as-received microstructure and tensile fracture surface were captured using JEOL-7100F. Transmission electron microscopy (TEM) was conducted using a JEOL-2100F field emission instrument operated at $U = 200 \text{ kV}$. The elemental distribution in the HEA ingot was investigated using a field emission electron probe micro analyzer (EPMA) (JXA-8530F).

3 Results

Figure 2a, b show the macroscopic images of the as-cast CoCrFeMnNi HEA block and SEM microstructures of different regions shown in Fig. 2a. Generally, large grains with a columnar structure are evident in all areas except in region ⑤ where chill-zone like structures are dominant. For columnar grains, the average grain length in the long axis is very high (at over $1000 \mu\text{m}$), whereas that in the short axis is approximately $400 \mu\text{m}$. In the regions from ① to ④, the growth direction of the columnar grain is largely parallel to the W_S direction, as shown in Fig. 2b. For the consistency of the experiment, tensile specimens were taken in the regions from ① to ④ and not in the chill-zone like areas i.e., ⑤ and ⑥. Figure 2c shows a high-resolution TEM image revealing the typical microstructure around the area close to the ④ region in Fig. 2a. A relatively low density of dislocations was observed. Moreover, a single-phase fcc structure without any special nanoparticles was confirmed by the selected area diffraction pattern presented in Fig. 2d.

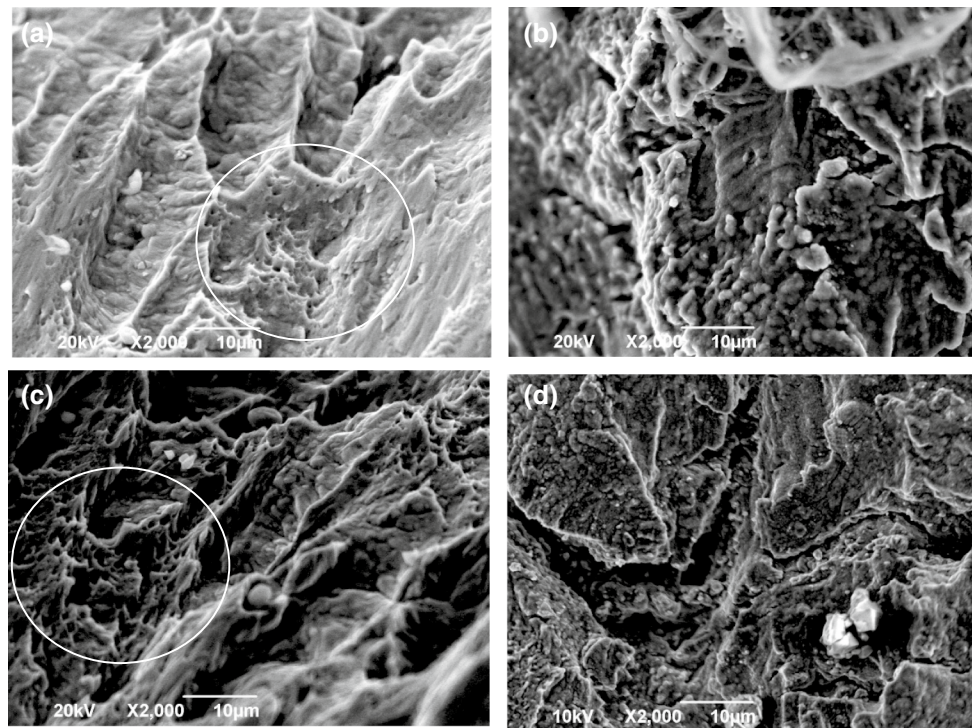


Fig. 4 Fracture surface of HEA samples loaded along different directions at **a, c** 22 °C and **b, d** 700 °C. Initial strain rate is 10^{-3} s^{-1} . White circles indicate the area of dimple structure

Figure 3 shows the representative engineering stress–strain curves with respect to the loading directions. At room temperature, the loading along the H direction exhibits higher ultimate tensile strength (UTS) and fracture elongation (E_f) than that along the W_s direction. However, at temperatures above 700 °C, the tensile anisotropy becomes less distinct. Regardless of the loading direction, high strength and ductility are observed at 22 and 500 °C, respectively. E_f is maximum at 500 °C for both samples. In contrast, at temperatures above 700 °C, both strength and ductility decrease remarkably. This result implies that a significant change in the deformation mechanism occurred between 500 °C and 700 °C. Figure 4 shows the fracture surfaces of the samples after tensile testing at 22 °C and 700 °C. The fracture surfaces of the room-temperature samples contain dimple structures, which are not observed in the samples tested at 700 °C. This result confirms that the deformation mechanisms at 22 °C and 700 °C are considerably different. The formation of dimple structures might have been due to twinning activity, which is suppressed at 700 °C. Without twinning, the thermally activated slip system may not help improve the ductility of the as-cast HEA.

On the other hand, serrations are observed on the stress–strain curves regardless of the loading direction at temperatures between 500 and 700 °C. When the

temperature reaches 800 °C, the serration disappears. Figure 5 shows the close-ups of the stress–strain curves at 500, 600, and 700 °C. Type-A like serrations, which exhibit upward serration above the general level of the stress–strain curve, are observed at a test temperature of 500 °C. The serration onset point is approximately at the strain level of 0.02. At 600 °C, a noticeable serration behavior extends from the yield point to the start of necking along all loading directions. The serration flow is random, and a combination of upward and downward stress drops is observed, indicating type-B serration. At 700 °C, the serration flow changes into downward stress drop, which is typical of type-C serration. The degree of serration is found to depend on the loading direction. For example, when loading along the W_s direction, the strain interval between the stress drops is highest, whereas the flat part is largely absent in the stress–strain curve along the H direction. Regardless of the temperature, the stress drop amplitude ($\Delta\sigma$) seems to be highest along the H direction, which will be discussed later.

4 Discussion

At relatively low temperatures of 500 °C, Type-A like serrations occurred, whereas type-B and type-C serrations were observed at 600 and 700 °C, respectively. The type-A

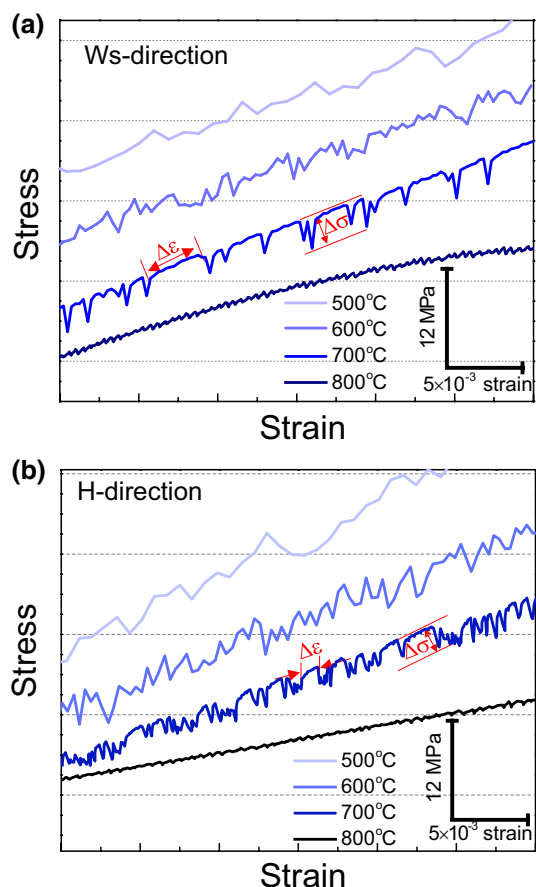


Fig. 5 Close-ups of stress–strain curves at a strain rate of 10^{-3} s^{-1} . The stress–strain curves at each temperature are arbitrarily shifted for intuitive comparison of the serration behavior. $\Delta\epsilon$ and $\Delta\sigma$ represent the strain increment required for another stress drop and stress drop amplitude, respectively

serrations occasionally observed at relatively low temperatures are dominated by the locking process of diffusing solute atoms, whereas the type-C serrations observed at high temperatures are due to the unlocking of the initially aged dislocations [17]. At high-temperature regimes, it is thought that the diffusion rates are high enough for the dislocations to be aged from the start of deformation. The type-C serrations are due to the breaking away of the aged dislocations [17]. In conventional alloys, the serrations, which are reminiscent of the PLC effect, are due to the diffusion of interstitial solute atoms, such as C and N, to the dislocations. The adherence of the solute atoms to dislocations increases the flow stress because of the pinning effect. Once the flow stress is increased by the continuous applied stress, the pinned dislocations can break away from the solute atmosphere and less stress is required for moving away [20]. In some cases, the interaction between the fine precipitate and the dislocation is assumed to cause serrated flow [21]. However, in

this study, no special nanoparticles, which can serve as a dislocation pinning source, were found in the high-resolution TEM observations (see Fig. 2c, d). Moreover, the concentrations of C and N are lower than those of conventional alloys exhibiting the serration behavior.

In contrast to the interstitial atoms, substitutional atoms are often big and occupy the normal lattice positions in the alloys. Nevertheless, just like for carbon steels, serrations often appear in some substitutional solution systems for certain environments due to the interaction between the solutes and the dislocations motion [22]. Recently, in fcc HEAs, Carroll et al. [19] demonstrated that the pinning of dislocations originates from abundant sources of solutes in the whole-solute matrix. Moreover, Fu et al. [18] calculated activation energies (Q) for serrated flow of CoCrFeNiMn HEA and found out that quite a high Q value of 296 kJ mol^{-1} was observed at temperatures ranging from 500 to 600 °C. This Q value is much higher than those ($76\text{--}103 \text{ kJ mol}^{-1}$) reported for the diffusion of interstitial solutes such as carbon in bcc iron and steels [23]. Further, the Q value for HEA is close to the lattice diffusion coefficient of the constituent elements in the CoCrFeNiMn alloy, i.e., Co (307 kJ mol^{-1}), Cr (293 kJ mol^{-1}), Fe (310 kJ mol^{-1}), Ni (318 kJ mol^{-1}), and Mn (288 kJ mol^{-1}) [24]. This result implies that the serration flow is strongly related to the cooperative lattice diffusion of the constituent elements. However, the high Q for the serrated flow might make it slightly difficult for solute atoms to diffuse and stick to dislocations. This result may decrease $\Delta\sigma$ of the present alloy and make it lower than those in interstitial solutes systems [25].

For active serration, an effective solute atmosphere requires a minimum concentration of solutes that can diffuse toward the mobile dislocations and lock them. In HEAs, the level of the solutes is over approximately 20 at%. Therefore, all the elements can effectively serve trapping solutes. The difference in the serration behaviors with respect to the loading direction might be due to the inhomogeneous distribution of each solute atom throughout the material. Ma et al. [26] suggested that Fe segregates to dendrites, while Mn and Ni segregate to inter-dendritic regions. The same segregation phenomenon is confirmed in the present material using the EPMA analysis, as shown in Fig. 6. With respect to the loading direction, the moving dislocations should have different probabilities of meeting the segregation zone. Because the serration behavior is highly sensitive to the chemical composition, the serration behavior anisotropy in the as-cast HEA can be explained via this scheme. For example, the tensile specimens machined along the H direction inherently contain higher number of dendrite cell boundaries than those machined along the Ws direction. Therefore, the probability of meeting the segregation zone must be

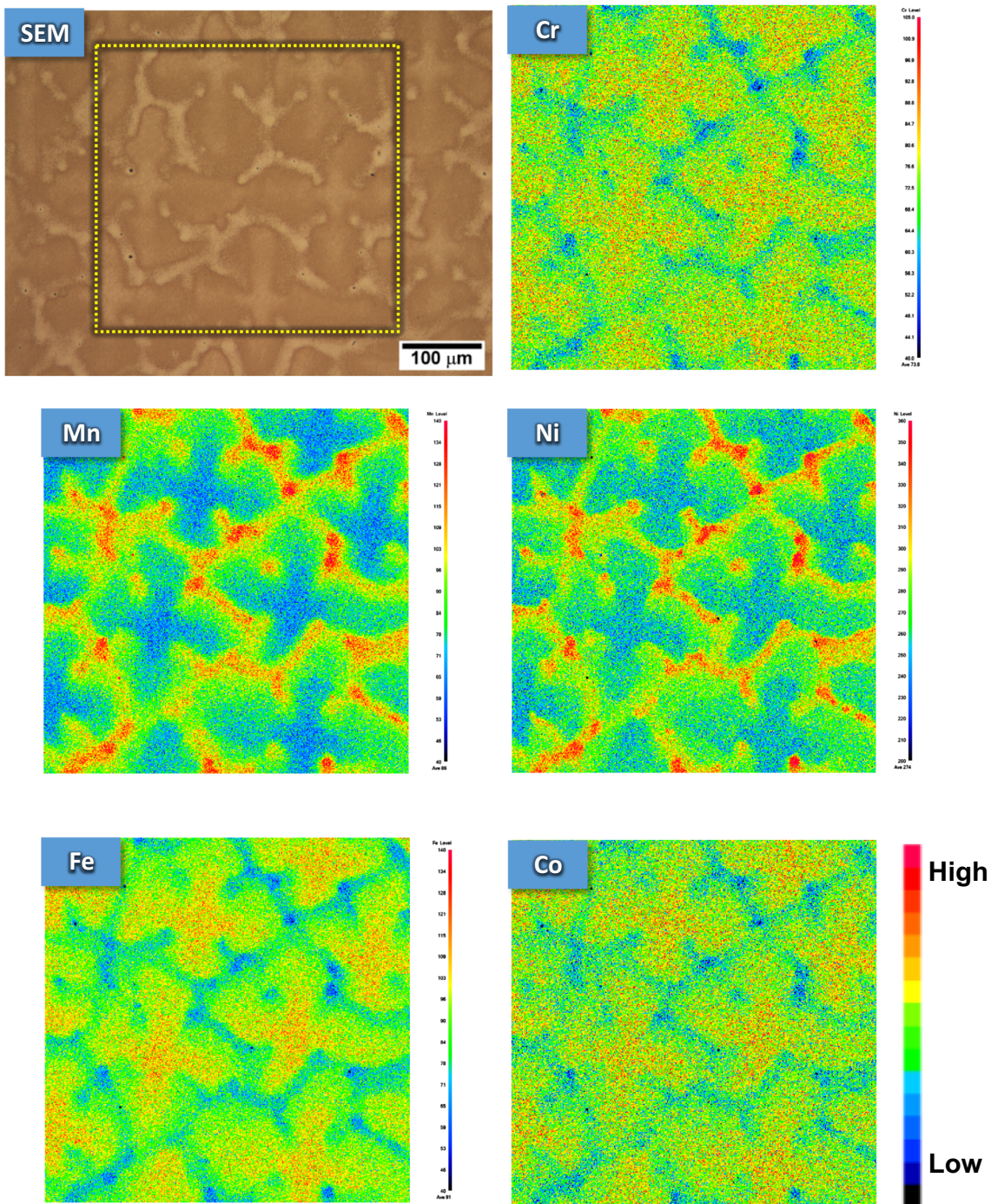


Fig. 6 EPMA elemental mapping (Cr, Mn, Ni, Fe, and Co) of the as-cast HEA sample. Segregation of Mn and Ni to the interdendritic regions is noticed

higher when loaded along the H direction. In practice, at 700 °C, the strain increment ($\Delta\epsilon$) required for another stress drop is significantly lower along the H direction than along other directions (see Fig. 5). The stress drop amplitude ($\Delta\sigma$) was calculated from the true stress versus strain data converted from the initial engineering stress and strain curves. Figure 7 shows the average $\Delta\sigma$ at 500

and 700 °C as a function of the strain. The average $\Delta\sigma$ is higher along the H direction than along the Ws direction. Regardless of the loading direction, the maximum amplitude of the stress drop is not very high (below 5.0 MPa). $\Delta\sigma$ increases with the increase in the strain up to a certain critical strain level. For example, at 500 °C, $\Delta\sigma$ is maximum at strain levels of 0.39 and 0.40 along the Ws and H

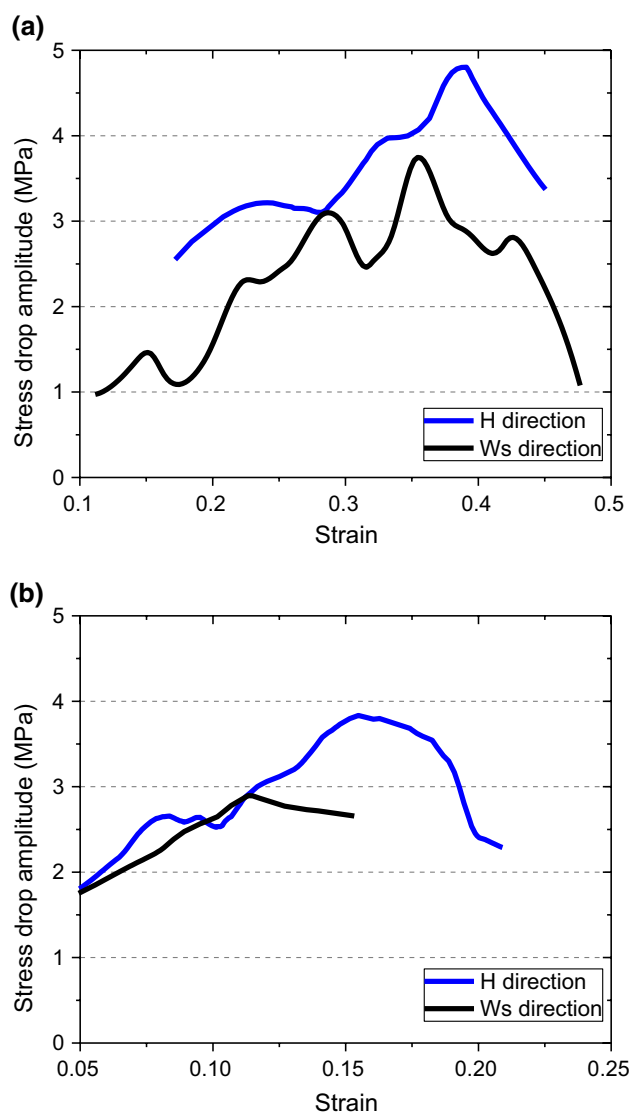


Fig. 7 Plots showing the stress drop amplitude ($\Delta\sigma$) at **a** 500 and **b** 700 °C. $\Delta\sigma$ is determined from the maximum stress prior to the beginning of the major stress drop to the minimum stress prior to the beginning of the major stress increase

directions, respectively, and thereafter decreases with the strain. Interestingly, the critical strain level of each sample is close to the strain hardening transition point (0.40 and 0.38 for Ws and H directions, respectively), where the strain hardening rate starts to decrease with the strain after passing the plateau region (see Fig. 4c in Ref. [27]). A similar behavior is observed at 700 °C as well. Because the stress drop is related to the plastic events, it is speculated that the relationship of $\Delta\sigma$ with the strain might be associated with the hardening behavior.

The serration behavior is generally associated with dynamic strain aging. Otto et al. [28] observed the serration behavior of wrought CoCrFeMnNi sheets at 400 °C

and nominal strain rate of 10^{-3} s^{-1} . Contrary to the present result, the serration behavior of wrought CoCrFeMnNi was not very distinct and it disappeared at temperatures above 600 °C. Carroll et al. [19] reported similar results showing that the serrated stress–strain curves move from type-A to B PLC-bands at 500 °C. Compared to the results obtained for wrought HEAs, the start and finish temperatures of serration are slightly higher in the as-cast HEA by 100–200 °C. Even above the temperature of 700 °C, the serration mechanisms may operate. However, all the serrations were washed out by thermal fluctuations [29], and the stress–strain curves became smooth, as shown in Fig. 5.

5 Conclusions

1. The tensile anisotropy of an as-cast CoCrFeMnNi HEA was observed at room temperature. The difference in the tensile strength and elongation was not significant at high temperatures. A noticeable serration behavior was observed during medium-to-high temperature tensile loading.
2. The start and finish temperatures of serration flow were slightly higher in the as-cast HEA by 100–200 °C compared to that in the wrought HEA. With the increase in the temperature from 500 to 700 °C, distinct serration flows occurred and evolved in the sequence of type-A, type-B, and type-C serrations. In contrast to conventional alloys, the serration flow seems to be related to the lattice diffusion of constituent elements.
3. The degree of serration was found to depend on the loading direction. At 700 °C, the average stress drop amplitude was higher along the H direction than along the Ws direction probably due to the higher probability of dislocations meeting the Mn and Ni segregation zone. Finally, the strain increment required for subsequent stress drops was significantly lower along the H direction.

Acknowledgements This research was supported by Creative Materials Discovery Program through the National Research Foundation of Korea (NRF) funded by Ministry of Science and ICT (NRF-2016M3D1A1023534). This work was also partially supported by a Grant from the National Research Foundation of Korea (NRF) funded by the Korean government (MSIT) (No. 2018R1A2B6004490).

References

1. Z. Li, S. Zhao, S.M. Alotaibi, Y. Liu, B. Wang, M.A. Meyers, *Acta Mater.* **151**, 424 (2018)
2. B. Gludovatz, A. Hohenwarter, D. Catoor, E.H. Chang, E.P. George, R.O. Ritchie, *Science* **345**, 1153 (2014)
3. D. Yim, H.S. Kim, *Korean J. Metals Mater.* **55**, 671 (2017)
4. M. Kang, J.W. Won, K.R. Lim, S.H. Park, S.M. Seo, Y.S. Na, *Korean J. Metals Mater.* **55**, 732 (2017)

5. Z. Wu, Y.F. Gao, H. Bei, *Scr. Mater.* **109**, 108 (2015)
6. J.Y. Ko, J.S. Song, S.I. Hong, *Korean J. Metals Mater.* **56**, 26 (2018)
7. A.J. Zaddach, R.O. Scattergood, C.C. Koch, *Mater. Sci. Eng., A* **636**, 373 (2015)
8. D.B. Miracle, O.N. Senkov, *Acta Mater.* **122**, 448 (2016)
9. S.W. Kim, J.H. Kim, *Mater. Sci. Eng., A* **718**, 321 (2018)
10. N.K. Adomako, J.H. Kim, Y.T. Hyun, *J. Therm. Anal. Calorim.* **133**, 13 (2018)
11. A. Gali, E.P. George, *Intermetallics* **39**, 74 (2013)
12. Y. Deng, C.C. Tasan, K.G. Pradeep, H. Springer, A. Kostka, D. Raabe, *Acta Mater.* **94**, 124 (2015)
13. Z. Wu, H. Bei, G.M. Pharr, E.P. George, *Acta Mater.* **81**, 428 (2014)
14. G.D. Sathiaraj, P.P. Bhattacharjee, *J. Alloys Compd.* **647**, 82 (2015)
15. M. Pozuelo, Y.W. Chang, J. Marian, J.M. Yang, *Scr. Mater.* **127**, 178 (2017)
16. Q. Hu, Q. Zhang, P. Cao, S. Fu, *Acta Mater.* **60**, 1647 (2012)
17. G.M. Han, C.G. Tian, Z.K. Chu, C.Y. Cui, Z.Q. Hu, X.F. Sun, *Metall. Mater. Trans. A Phys. Metall. Mater. Sci.* **46**, 4629 (2015)
18. J.X. Fu, C.M. Cao, W. Tong, Y.X. Hao, L.M. Peng, *Mater. Sci. Eng., A* **690**, 418 (2017)
19. R. Carroll, C. Lee, C.-W. Tsai, J.-W. Yeh, J. Antonaglia, B.A.W. Brinkman, M. LeBlanc, X. Xie, S. Chen, P.K. Liaw, K.A. Dahmen, *Sci. Rep.* **5**, 16997 (2015)
20. S. Chen, X. Xie, W. Li, R. Feng, B. Chen, J. Qiao, Y. Ren, Y. Zhang, K.A. Dahmen, P.K. Liaw, *Mater. Chem. Phys.* **210**, 20 (2018)
21. D. Thevenet, M. Mliha-Touati, A. Zeghloul, *Mater. Sci. Eng., A* **266**, 175 (1999)
22. K. Chihab, C. Fressengeas, *Mater. Sci. Eng., A* **356**, 102 (2003)
23. B.K. Choudhary, *Mater. Sci. Eng., A* **564**, 303 (2013)
24. K.Y. Tsai, M.H. Tsai, J.W. Yeh, *Acta Mater.* **61**, 4887 (2013)
25. Y. Zhang, J.P. Liu, S.Y. Chen, X. Xie, P.K. Liaw, K.A. Dahmen, J.W. Qiao, Y.L. Wang, *Prog. Mater. Sci.* **90**, 358 (2017)
26. D. Ma, M. Yao, K.G. Pradeep, C.C. Tasan, H. Springer, D. Raabe, *Acta Mater.* **98**, 288 (2015)
27. J.H. Kim, K.R. Lim, J.W. Won, Y.S. Na, H.-S. Kim, *Mater. Sci. Eng., A* **712**, 108 (2018)
28. F. Otto, A. Dlouhý, C. Somsen, H. Bei, G. Eggeler, E.P. George, *Acta Mater.* **61**, 5743 (2013)
29. F.A. Mohamed, K.L. Murty, T.G. Langdon, *Acta Metall.* **22**, 325 (1974)